

# Highly ordered horizontal indium gallium arsenide/indium phosphide multi-quantum-well in wire structure on (001) silicon substrates

Yu Han, Qiang Li, and Kei May Lau

Citation: *J. Appl. Phys.* **120**, 245701 (2016); doi: 10.1063/1.4972481

View online: <http://dx.doi.org/10.1063/1.4972481>

View Table of Contents: <http://aip.scitation.org/toc/jap/120/24>

Published by the [American Institute of Physics](#)

---

---

# Highly ordered horizontal indium gallium arsenide/indium phosphide multi-quantum-well in wire structure on (001) silicon substrates

Yu Han,<sup>a)</sup> Qiang Li,<sup>a)</sup> and Kei May Lau<sup>b)</sup>

*Department of Electronic and Computer Engineering, Hong Kong University of Science and Technology, Clear Water Bay, Kowloon, Hong Kong*

(Received 25 September 2016; accepted 6 December 2016; published online 22 December 2016)

We report the characteristics of indium gallium arsenide stacked quantum structures inside planar indium phosphide nanowires grown on exact (001) silicon substrates. The morphological evolution of the indium phosphide ridge buffers inside sub-micron trenches has been studied, and the role of inter-facet diffusion in this process is discussed. Inside a single indium phosphide nanowire, we are able to stack quantum structures including indium gallium arsenide flat quantum wells, quasi-quantum wires, quantum wires, and ridge quantum wells. Room temperature photoluminescence measurements reveal a broadband emission spectrum centered at 1550 nm. Power dependent photoluminescence analysis indicates the presence of quasi-continuum states. This work thus provides insights into the design and growth process control of multiple quantum wells in wire structures for high performance nanowire lasers on a silicon substrate with 1550 nm band emission. *Published by AIP Publishing.* [<http://dx.doi.org/10.1063/1.4972481>]

## I. INTRODUCTION

Replacing electrical wires with optical interconnects is expected to alleviate the intra and inter-chip communication bottleneck encountered by present silicon(Si)-based micro-processors.<sup>1,2</sup> Instead of incorporating inefficient Si-based light emitters, implementation of group III–V active layers onto Si substrates for light emission is being extensively investigated.<sup>3–5</sup> Epitaxial growth of III–V nanowires and nanostructures on Si can potentially overcome the fundamental challenges in material mismatch. Besides, the large reflective index contrast with the ambient and the distinct wire geometry lead to intrinsic Fabry-Perot cavities that can sustain axially guided optical modes. So far, lasing operation has been reported in gallium arsenide (GaAs), indium phosphide (InP), indium gallium arsenide (InGaAs), and gallium antimonide (GaSb) based nanowires.<sup>6–12</sup> However, these nanowire lasers feature either a cleavage and transfer process to obtain enhanced optical confinement or a vertical configuration that is not fully compatible with the planar process in complementary metal–oxide–semiconductor (CMOS) manufacturing. Recently, progress in selective area growth (SAG) of high mobility III–V channel materials on pre-patterned (001) Si for advanced CMOS has motivated the exploration of a III–V/Si photonics platform in a similar manner.<sup>13–16</sup> An optically pumped room-temperature distributed feedback laser array using bulk InP monolithically grown on (001)-silicon was recently demonstrated.<sup>17</sup> However, compared to bulk materials with limited gain, quantum structures with modified density of states (DOS) are preferred to obtain low threshold and improve temperature stability. Moreover, extending the lasing wavelength to 1550 nm would open enormous opportunities for on-chip communications.

Previously, we reported single InGaAs quasi-quantum wire embedded inside InP nanowires on (001) Si emitting in the 1550 nm communication band.<sup>18</sup> Here, through detailed transmission electron microscope (TEM) investigation of the facet evolution of InP nanowires inside sub-micron trenches on Si, we are able to demonstrate InGaAs/InP multi-quantum-wells in wire structures with enhanced optical properties. In the past, there have been extensive theoretical studies on the mechanism of facet evolution in SAG processes on nonplanar substrates based on the self-limiting growth profile.<sup>19–21</sup> Various low dimensional III–V nanostructures have also been experimentally explored, such as flat and ridge quantum wells inside sub-micron trenches,<sup>15,22–24</sup> V-groove and ridge quantum wires.<sup>25–30</sup> However, experimental study of facet evolution of planar InP nanowires inside sub-micron trenches on (001) Si is still lacking. In this work, using inserted InGaAs multi-quantum wells as growth markers, we discovered a transient behavior of the (001) facet in the InP ridge structure, which is found related to the contact of the InP (111) plane with the SiO<sub>2</sub> spacer sidewalls. This allows us to obtain various InGaAs quantum structures inside the InP nanowires, including flat quantum wells, quasi-quantum wires, quantum wires, and ridge quantum wells. This study here thus provides important insights into the design and fabrication of long-wavelength nanowire lasers on exact (001) Si substrates.

## II. MATERIAL GROWTH

We grew the InP nanowires and embedded multi-InGaAs quantum structures on stripe patterned (001) p-type Si substrates (150 nm thick SiO<sub>2</sub>, 800 nm line pitch, and 300 nm openings) using a metal-organic chemical vapor deposition (MOCVD) system with a horizontal reactor (AIXTRON 200/4). The sub-micron trenches were aligned along the [110] direction. Diamond shaped pockets enclosed

<sup>a)</sup>Y. Han and Q. Li contributed equally to this work.

<sup>b)</sup>Email: eekmlau@ust.hk. Tel.: (852)23587049. Fax: (852) 23581485.

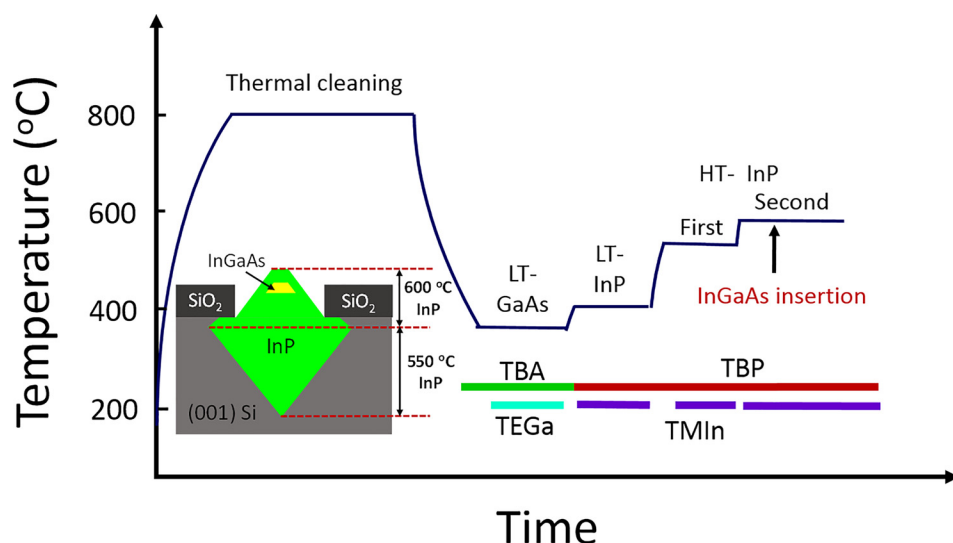


FIG. 1. Schematic showing the detailed growth procedure of the InP nanowire on Si. Inset displays positions of two HT-InP growth stages.

by Si {111} surfaces were formed through KOH anisotropic wet etching (45% concentration at 70 °C) to achieve single domain growth and thus to avoid the formation of anti-phase boundaries (APBs). The growth is schematically summarized in the temperature vs time profile shown in Fig. 1. After a thermal cleaning procedure at 800 °C to desorb the residual native oxide at surfaces of the Si enclosure, a low temperature (LT) GaAs nucleation layer was deposited at 400 °C using triethylgallium (TEGa) as the group-III precursor and tertiarybutylarsine (TBA) as the group-V precursor. This ultra-thin GaAs nucleation layer provides a good coverage of the initial Si surfaces and serves as a strain reduction buffer for the subsequent InP growth. A three-step InP growth procedure was adopted in our experiment. First, the LT-InP nucleation layer was grown at 450 °C with trimethylindium (TMIn) and tertiarybutylphosphine (TBP) as group-III and V precursors, respectively. Then, the reactor temperature was ramped up to 550 °C. Growth of InP at this temperature continued until the InP layer was flush with the Si (111) corner as indicated by the red line in the inset of Fig. 1. The remaining InP layer together with the inserted InGaAs quantum structures was carried out at 600 °C.

### III. RESULTS AND DISCUSSION

Scanning electron microscope (SEM) analysis was carried out to study the morphological evolution of the InP nanowires at different growth stages. Fig. 2(a) displays a 70° tilted-view SEM image of the initial LT- GaAs nucleation

layer at the (111) Si sidewalls, indicating the formation of high density islands along the sloped Si surface as shown by the green dotted line. A high resolution TEM image of the V-groove bottom after the InP/GaAs growth is presented in Fig. 2(b). The large GaAs/Si lattice mismatch was accommodated by a few layers of stacking faults. Fig. 3(a) reveals the surface morphology of the InP nanowires after the 550 °C layer growth, with an uneven surface resulting from the coalescence of the initial InP islands. InP clusters were formed during the LT-InP nucleation stage and these clusters would further develop into large InP islands during the HT-InP growth.<sup>31</sup> Continued growth would lead to the inevitable coalescence of the large InP islands confined in the trenches. Note that the slight pattern tilting in Fig. 3(a) is an artifact of the SEM imaging. Fig. 3(b) displays the semi-rhombic shaped InP nanowires after the 600 °C deposited InP, showing flat (001) top facets and smooth (111) side facets. As growth was prolonged in Fig. 3(c), the {111} sidewalls of InP started to contact the SiO<sub>2</sub> sidewall.

We inserted multiple InGaAs quantum structures after formation of the InP ridges. Cross-sectional TEM images of one sample (QS-1) recorded from the plane perpendicular to the nanowire array are shown in Fig. 4. Fig. 4(a) showing the entire wire in the pocket illustrates that most of the defects generated at the III-V/Si interface are confined within the lower diamond-shaped pocket, while the upper position of the InP nanowire is less defective. Figs. 4(b)–4(d) present zoomed-in TEM images of the four InGaAs quantum structures. The InGaAs layers exhibit crescent shape due to the

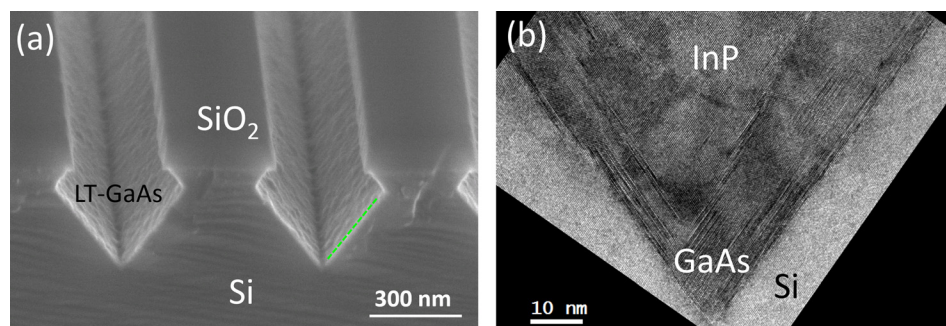


FIG. 2. (a) 70° tilted-view SEM image of the LT-GaAs layer on the initial Si (111) surfaces, showing the complete coverage. (c) High resolution TEM image of the initial LT-GaAs layer on the Si enclosure after the InP nanowire growth.

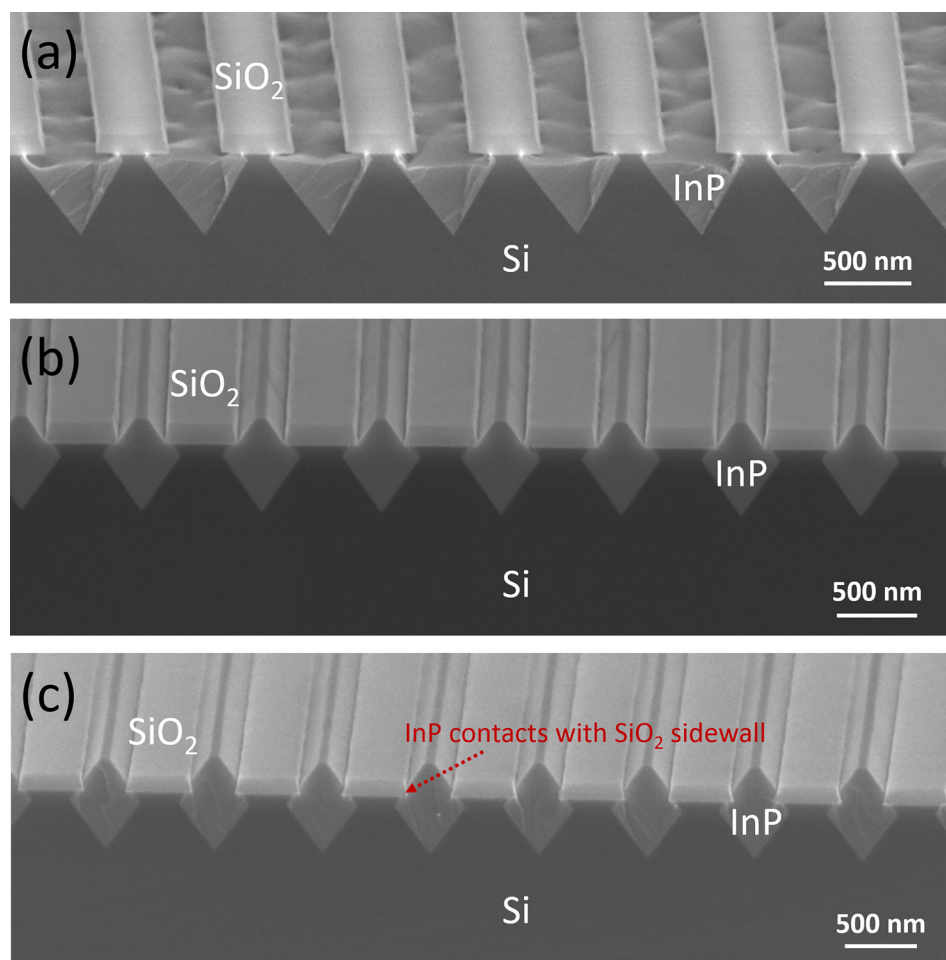


FIG. 3. (a) SEM image of the InP nanowire after the first HT-InP layer. Surface fluctuation indicates the coalescence of the InP islands. (b) SEM image of the InP nanowire after the second HT-InP layer, showing semi-rhombic geometry and flat facets. (c) InP nanowire after prolonged growth time, indicating deviation from rhombic shape and contact between (111) plane InP and the SiO<sub>2</sub> sidewall.

presence of nonplanar facets. From bottom to top, we observe a transition of the InGaAs insert from quantum wells to quasi-quantum wires with decreasing lateral dimensions. In the meantime, the stacked InGaAs layers serve as excellent markers for the interpretation of the facet evolution during the SAG process. While the size of (111) facets kept increasing, a different trend was observed for the (001) facet. From the bottom quantum well to the top quasi-quantum wire, the (001) facet decreases in the lateral dimension until complete disappearance. The minimization of the (001) facet in this stage is to avert direct contact with SiO<sub>2</sub> sidewalls and thus minimize the total surface energy. After the upper most InGaAs quasi-quantum wire was formed, subsequent growth led to inevitable contact of the InP with the SiO<sub>2</sub> sidewalls. Since the surface energy of the (001) facet is smaller than that of the (111) facet, the inclination to minimize total surface energy at this stage leads to the reappearance of (001) facet. The size of the (001) facet would keep increasing until reaching the final self-limiting shape.

During the SAG, both inter-facet diffusion and external flux contribute to the facet evolution. Since external flux was kept constant during the whole growth process, the diffusion of adatoms under the same growth pressure and temperature was also identical. We believe that the difference in inter-facet diffusion led to the vanishing and reappearance of the (001) facet. As shown in Fig. 4(e), before the InP (111) plane was in contact with the SiO<sub>2</sub> sidewalls, adatoms diffused

from the (111) facet to the (001) facet, resulting in a higher growth rate of the (001) facet and therefore a decreasing facet size. With continued growth, after filling up the pocket and InP contacting with SiO<sub>2</sub> spacer, the InP/SiO<sub>2</sub> interfacial energy began to contribute to the total surface energy. The direction of inter-facet diffusion reverses, leading to the re-emerging of the (001) facet and subsequent increasing facet size.

To investigate further, we postponed the insertion of the stacked InGaAs wells in another sample (QS-2), to study the growth behavior after the added effects of the interfacial energy. The cross-sectional TEM images from QS-2 are shown in Fig. 5. Four InGaAs quantum structures can be clearly identified, with the first two formed before and the last two after the involvement of InP/SiO<sub>2</sub> interfacial energy. The involvement of the interfacial energy was evidenced by examining the contact between the (111) ridge quantum well and the SiO<sub>2</sub> sidewall. As seen in Fig. 5(b), the InP barrier between the second and third InGaAs quantum structure is 76 nm high along the [001] direction and less than 2 nm wide along the [111] direction, implying a huge preference of growth on the (001) plane over the (111) plane. On the contrary, the final InP cap layer is 4 nm high along the [001] direction and 20 nm wide along the [111] direction. The reversed growth preference for different facets further substantiates our previous discussion on the role of interfacial energy and inter-facet diffusion.

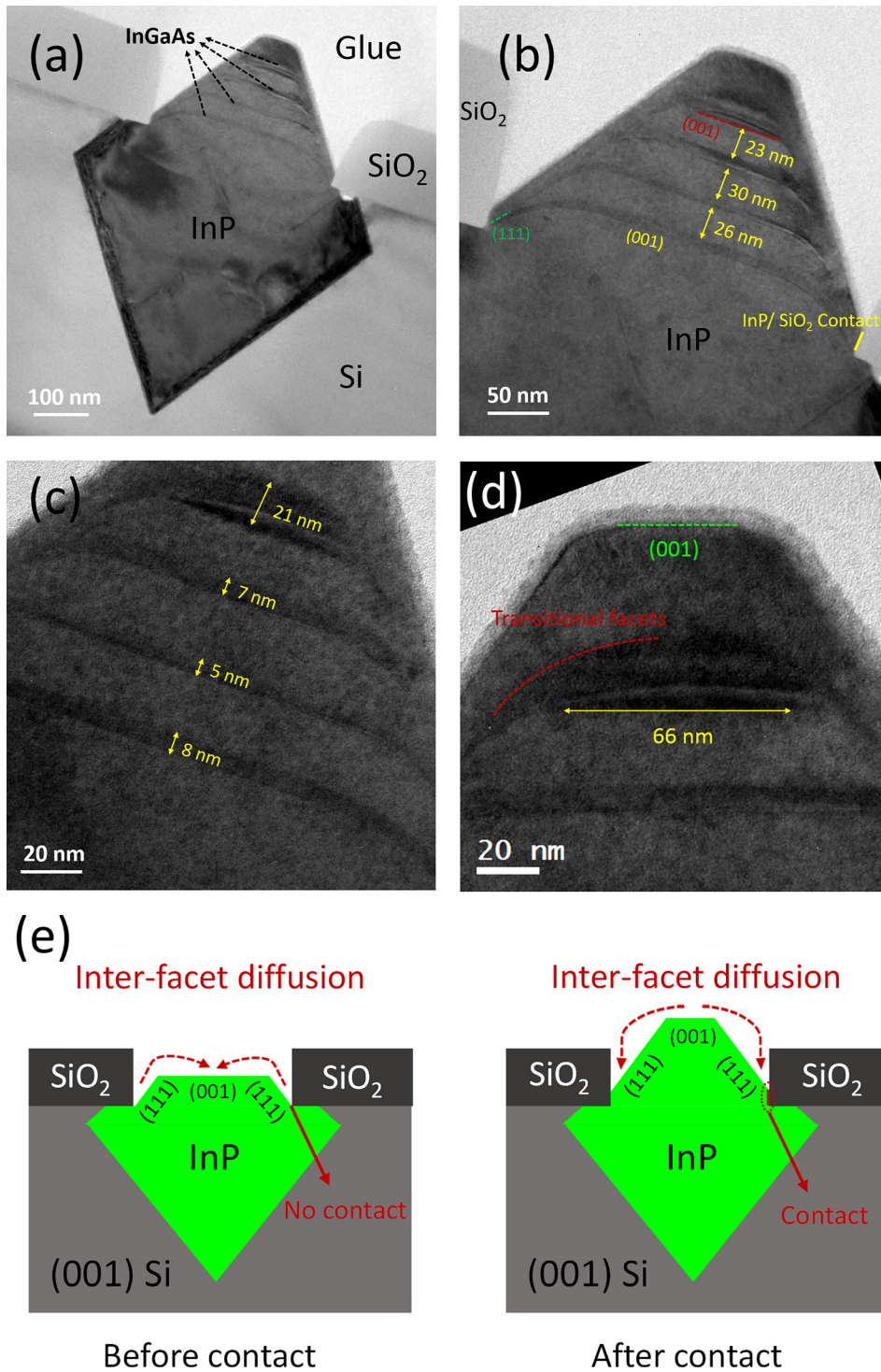


FIG. 4. (a) Cross sectional TEM image of the InP nanowire with inserted InGaAs quantum structures (QS-1) (b) Zoomed-in TEM image, showing the details of the quantum structures. Thickness of InP interlayer is labeled (c) Zoomed-in TEM image of the center of the quantum structures with thickness marked. (d) High resolution TEM image of the top InGaAs quasi-quantum wire, indicating the complete disappearance and reemerging of (001) facet. (e) Schematic of the inter-facet diffusion before and after (111) plane InP contacts with SiO<sub>2</sub> sidewall.

Fig. 5(c) presents a zoomed-in view of the last two InGaAs quantum structures in QS-2. Crescent-shaped InGaAs quantum wire was obtained with a thickness of 8 nm and a width of 20 nm near the top of the wire. A 2 nm InGaAs ridge quantum well was formed simultaneously along the (111) facet. We expect a lower indium fraction at the junction of the crescent quantum wire and the ridge quantum well, since indium adatoms are inclined to escape from high curvature regions.<sup>19</sup> Therefore, quantum confinement from both vertical and lateral directions is expected for the center region of the quantum wire. Fig. 6 presents a zoomed-in TEM image of

these ridge InGaAs quantum wells. Four ridge quantum wells can be clearly observed with increasing length and decreasing thickness. Up to this point, we have been able to grown various InGaAs quantum structures at different positions of the InP nanowire. The transition from the quantum well, to the quasi-quantum wire, and finally to the quantum wire is clearly evidenced by the TEM characterization. The evolution of facet size and the change in growth rate are summarized in Figs. 7(a) and 7(b), respectively. The facet sizes of both (001) and (111) facets were measured using the presented high resolution TEM images. As discussed earlier, the trend in both

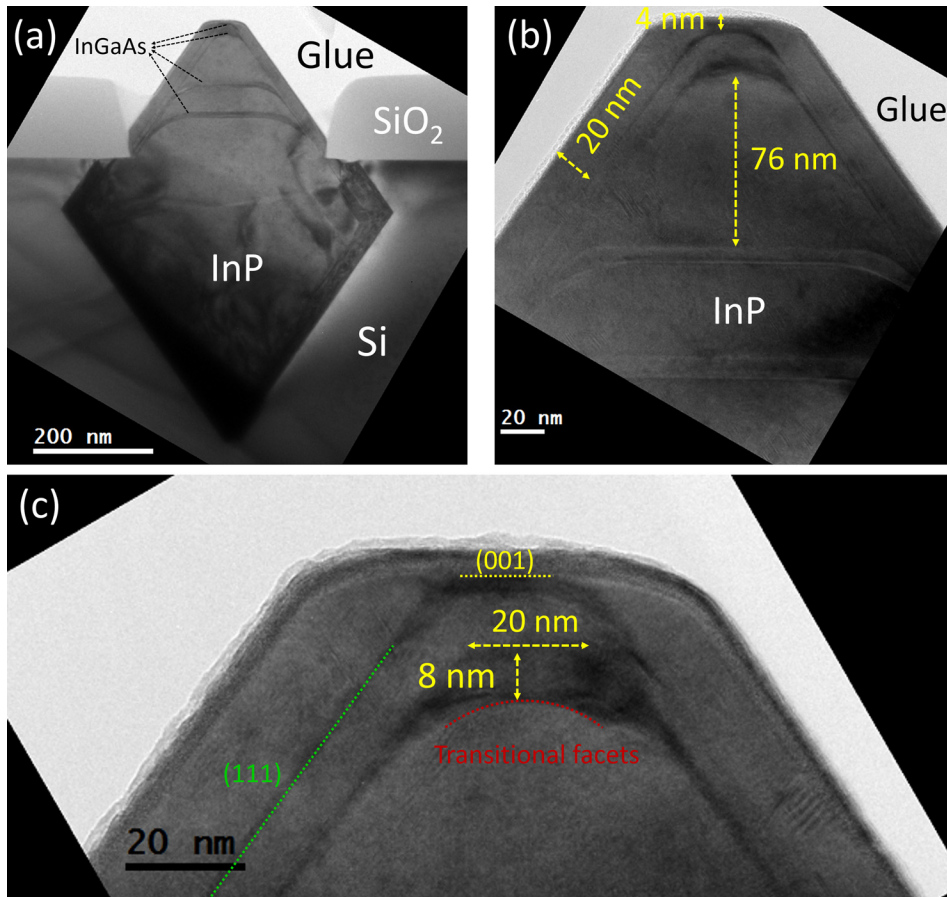


FIG. 5. (a) Cross sectional TEM image of the InP nanowire with four embedded InGaAs quantum structures (QS-2). (b) Zoomed-in TEM image, showing the details of the quantum structures. Thickness of the InP interlayer is labeled. (c) High resolution TEM image of the InGaAs quantum wire with 8 nm thickness and 20 nm width.

facet size and growth rate would reverse when the InP (111) plane contacts the SiO<sub>2</sub> sidewall. Note that the growth rate of (111) plane InP drops slightly, as indicated in Fig. 7(b). This could be due to the increase of overall growth surface area while external flux was kept constant.

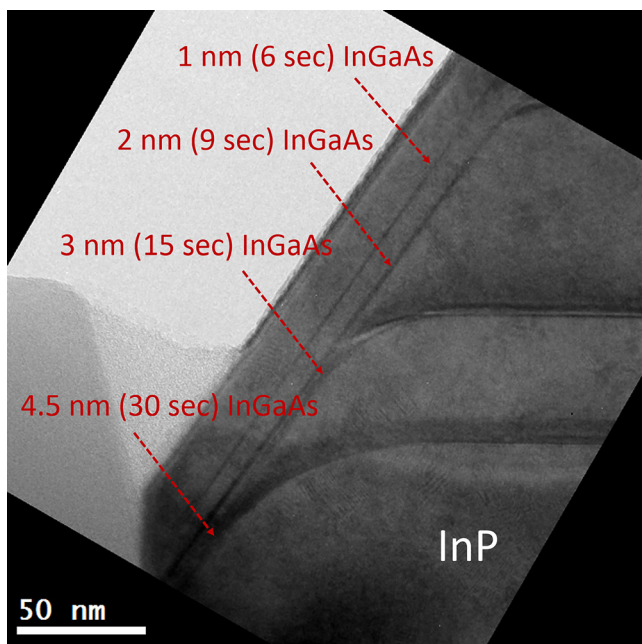


FIG. 6. High resolution TEM image of the ridge InGaAs quantum wells along the (111) direction. Thickness is labeled.

The optical properties of these quantum structures were investigated through room-temperature macro-PL measurements using a laser source emitting at 671 nm (spot size around 100  $\mu\text{m}$  in diameter) and a germanium detector. During each measurement, about 125 InP nanowires were excited and the obtained PL spectrum represented the collective PL signal of these 125 InP nanowires. Fig. 8(a) displays the PL spectra measured at 0.75 mW laser power. The central emitting wavelengths of the two stacked quantum structures (QS-1 and QS-2) are all situated at 1550 nm. A broad PL spectrum was obtained due to the inhomogeneity of both thickness and indium fraction. Besides, the interface fluctuation and uneven indium distribution might lead to localization of carriers and render a quantum-dot like behavior, which would further broaden the emission spectrum. A schematic of the conduction band minimum and valance band maximum in different regions of the quantum structures leading to the spontaneous emission process is sketched in Fig. 8(b). The central region of the quantum wire has a lower conduction band minimum, resulting from a larger wire thickness and a higher indium fraction. Theoretically, the density of states of quantum wires with strong quantum confinement from both vertical and lateral directions exhibits spike-like shape. However, in this case, we expect a quasi-continuum density of states in these quantum structures due to the overlapping states, as indicated in Fig. 8(c).<sup>32</sup>

Power dependent PL measurements have been performed for both samples QS-1 and QS-2. Figs. 9(a)–9(c) plot the integrated PL intensity, full width at half maximum

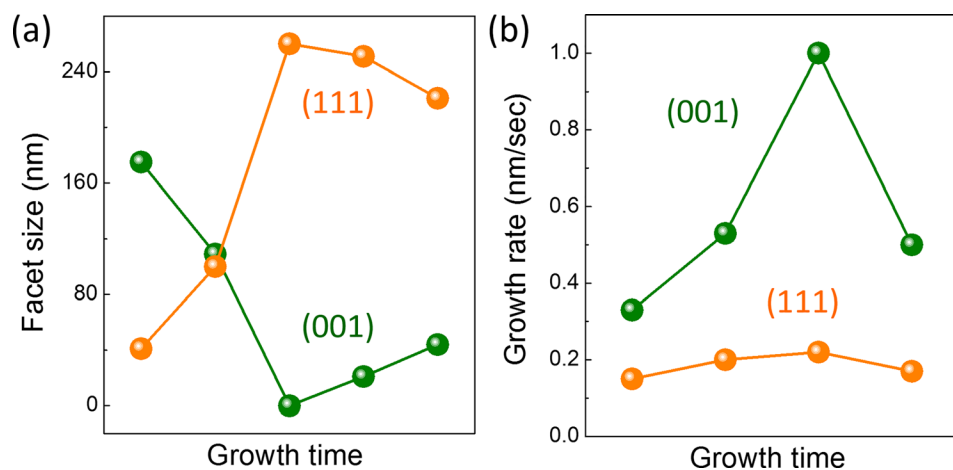


FIG. 7. (a) Facet size and (b) growth rate (InGaAs) of (001) and (111) facets at different growth stages.

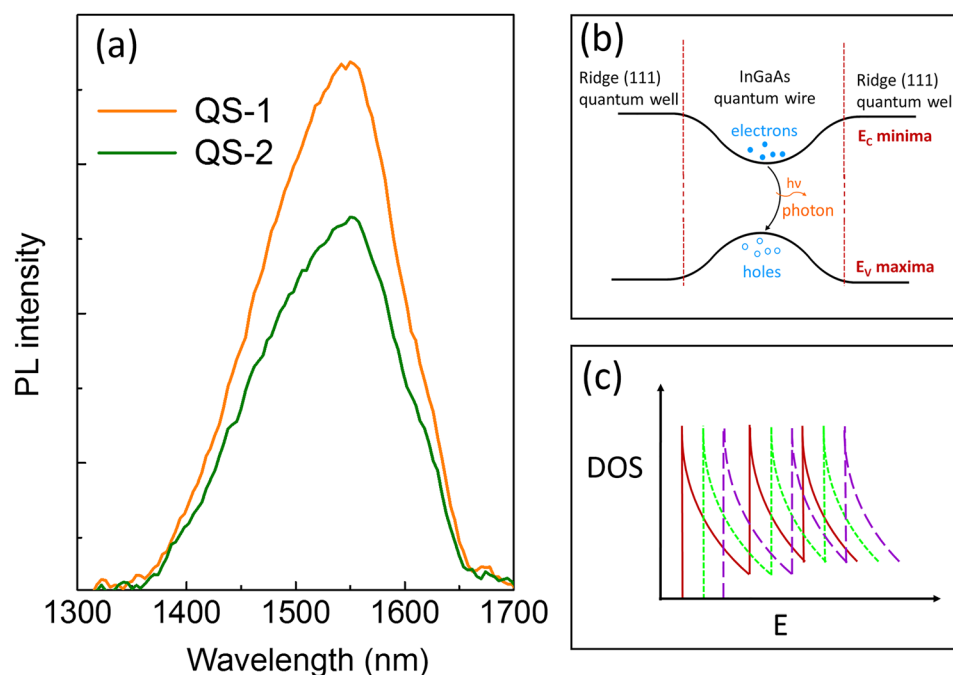


FIG. 8. (a) Room temperature PL spectrum of the two stacked InGaAs quantum structures. (b) Schematic shows the conduction band minima of the InGaAs quantum structure and (c) the overlapping of density of states due to thickness and composition inhomogeneity.

(FWHM), and central emitting wavelength as a function of the incident excitation laser power, respectively. A monotonic increase of integrated PL intensity can be observed as the excitation power increases and no apparent difference between QS-1 and QS-2 was detected. This indicates that the difference in the defect densities of these two quantum structures is negligible, since the influence of defect levels on the

integrated PL intensity is power dependent.<sup>33</sup> As shown in Fig. 9(b), a broadening of the line-width was observed when the pump power increases. In the multi-InGaAs quantum structures, the central region of the quantum wire serves as a “sink” of the excited carriers. At high incident power density, recombination of higher energy carriers from the edge region and ridge quantum wells resulted in the broadened

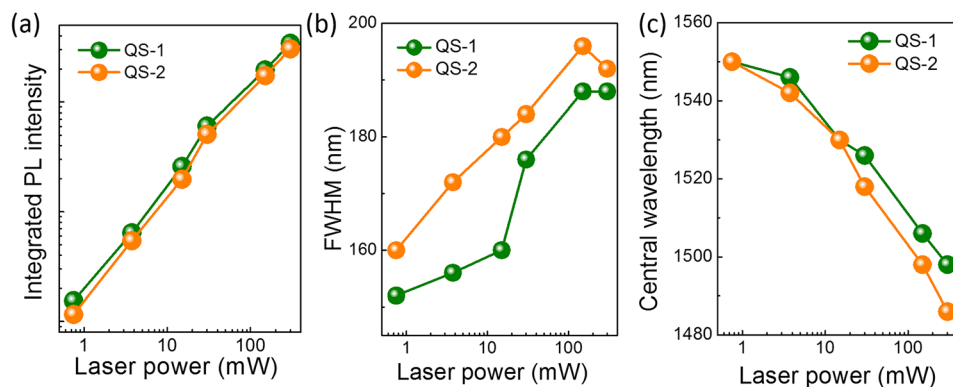


FIG. 9. (a) Power dependent measurement showing integrated PL intensity of the two quantum structures (QS-1 and QS-2). (b) The relationship of FWHM with pumping power. (c) Central wavelength shift during power dependent measurement.

emission spectrum. Owing to the larger degree of thickness inhomogeneity and larger size of ridge quantum wells, the FWHM of QS-2 is greater than that of QS-1 at all incident powers. The emission from higher energy levels also led to a blue shift of the central emitting wavelength, as evidenced by Fig. 9(c). For the eventual application as laser sources compatible with the COMS process, the FWHM of the PL spectrum should be reduced. Possible paths include ensuring identical thickness for the inserted InGaAs layers, elevating the insertion position for better defect necking effect, and tuning the growth parameters to improve the crystalline quality of the InP buffer layer.

#### IV. CONCLUSIONS

In conclusion, we have demonstrated the growth of highly ordered horizontal InGaAs/InP multi-quantum-wells in wire structures on exact (001) Si substrates. The morphological evolution of the InP nanowires inside sub-micro trenches was carefully examined through detailed SEM and TEM analysis. We observed the complete disappearance and reappearance of the (001) facet related to the emergence of III-V/sidewall interfacial energy. Various InGaAs quantum structures were thus formed inside a single InP nanowire. Power dependent PL measurements indicate potentially useful optical properties at the 1550 nm communication band. This result provides an excellent material basis for the fabrication of high performance nanowire lasers onto a (001) Si platform.

#### ACKNOWLEDGMENTS

This work was supported in part by Grant (Nos. 614813 and 16212115) from the Research Grants Council of Hong Kong. The authors would like to thank Shih-Pang Chang and Wen-Da Hsu from NDL for providing the patterned Si substrates and the MCPF of HKUST for technical support. Helpful discussions with C. W. Tang, C. Liu, B. Shi, and Y. Y. Chen are also acknowledged.

<sup>1</sup>Z. P. Zhou, B. Yin, and J. Michel, *Light: Sci. Appl.* **4**(11), 358 (2015).

<sup>2</sup>D. Lang and J. E. Bowers, *Nat. Photonics* **4**, 511 (2010).

<sup>3</sup>A. L. Liu, C. Zhang, J. Norman, A. Snyder, D. Lubyshev, J. M. Fastenau, A. W. K. Liu, A. C. Gossard, and J. E. Bowers, *Appl. Phys. Lett.* **104**, 041104 (2014).

<sup>4</sup>S. M. Chen, W. Li, J. Q. Wu, M. C. Tang, S. Shutts, S. N. Elliott, A. Sobiesierski, A. J. Seeds, I. Ross, P. M. Smowton, and H. Y. Liu, *Nat. Photonics* **10**, 307–311 (2016).

<sup>5</sup>Y. Wan, Q. Li, A. Y. Liu, A. C. Gossard, J. E. Bowers, E. L. Hu, and K. M. Lau, *Opt. Lett.* **41**(7), 1664 (2016).

<sup>6</sup>R. Chen, T.-T. D. Tran, K. W. Ng, W. S. Ko, L. C. Chuang, F. G. Sedgwick, and C. Chang-Hasnain, *Nat. Photonics* **5**, 170 (2011).

<sup>7</sup>D. Saxena, S. Mokkapati, P. Parkinson, N. Jiang, Q. Gao, H. H. Tan, and C. Jagadish, *Nat. Photonics* **7**, 963 (2013).

<sup>8</sup>B. Mayer, L. Janker, B. Loitsch, J. Treu, T. Kostenbader, S. Lichtmanecker, T. Reichert, S. Morkötter, M. Kanibler, G. Abstreiter, C. Gies, G. Koblmüller, and J. J. Finley, *Nano Lett.* **16**, 152 (2016).

<sup>9</sup>Y. Tatebayashi, S. Kako, J. Ho, Y. Ota, S. Iwamoto, and Y. Arakawa, *Nat. Photonics* **9**, 501 (2015).

<sup>10</sup>T. Stettner, P. Zimmermann, B. Loitsch, M. Döblinger, A. Regler, B. Mayer, J. Winnerl, S. Matich, H. Riedl, M. Kaniber, G. Abstreiter, G. Koblmüller, and J. J. Finley, *Appl. Phys. Lett.* **108**, 011108 (2016).

<sup>11</sup>A. H. Chin, S. Vaddiraju, A. V. Maslov, C. Z. Ning, M. K. Sunkara, and M. Meeyappan, *Appl. Phys. Lett.* **88**, 163115 (2006).

<sup>12</sup>Z. Wang, B. Tian, M. Paladugu, M. Pantouvaki, N. Le Thomas, C. Merckling, W. Guo, J. Dekoster, J. Van Campenhout, P. Absil, and D. Van Thourhout, *Nano Lett.* **13**, 5063 (2013).

<sup>13</sup>J. Z. Li, J. Bai, J.-S. Park, B. Adekore, K. Fox, M. Carroll, A. Lochtefeld, and Z. Shellenbarger, *Appl. Phys. Lett.* **91**, 021114 (2007).

<sup>14</sup>M. Paladugu, C. Merckling, R. Loo, O. Richard, H. Bender, J. Dekoster, W. Vandervorst, M. Caymax, and M. Heyns, *Cryst. Growth Des.* **12**(10), 4696 (2012).

<sup>15</sup>S. Li, X. Zhou, M. Li, X. Kong, J. Mi, M. Wang, W. Wang, and J. Pan, *Appl. Phys. Lett.* **108**, 021902 (2016).

<sup>16</sup>C. Merckling, N. Waldron, S. Jiang, W. Guo, N. Collaert, M. Caymax, E. Vancoille, K. Barla, A. Thean, M. Heyns, and W. Vandervorst, *J. Appl. Phys.* **115**, 023710 (2014).

<sup>17</sup>Z. C. Wang, B. Tian, M. Pantouvaki, W. M. Guo, P. Absil, J. V. Campenhout, C. Merckling, and D. V. Thourhout, *Nat. Photonics* **9**(12), 837–842 (2015).

<sup>18</sup>Y. Han, Q. Li, S. P. Chang, W. D. Hsu, and K. M. Lau, *Appl. Phys. Lett.* **108**, 242105 (2016).

<sup>19</sup>G. Biasiol, A. Gustafsson, K. Leifer, and E. Kapon, *Phys. Rev. B.* **65**, 205306 (2002).

<sup>20</sup>S. Jiang, C. Merckling, W. Guo, and N. Waldron, *J. Appl. Phys.* **115**, 023517 (2014).

<sup>21</sup>S. Li, X. Zhou, X. Kong, M. Li, J. Mi, and J. Pan, *J. Cryst. Growth.* **426**, 147–152 (2015).

<sup>22</sup>R. Cipro, T. Baron, M. Martin, J. Moeyaert, S. David, V. Gorbenko, F. Bassani, Y. Bogumilowicz, J. P. Barnes, N. Rochat, V. Loup, C. Vizioz, N. Allouti, N. Chauvin, X. Y. Bao, Z. Ye, J. B. Pin, and E. Sanchez, *Appl. Phys. Lett.* **104**, 262103 (2014).

<sup>23</sup>Q. Li, Y. Han, X. Lu, and K. M. Lau, *IEEE Electron Device Lett.* **37**, 24–27 (2016).

<sup>24</sup>B. Kunert, W. Guo, Y. Mols, B. Tian, Z. Wang, Y. Shi, D. Van Thourhout, M. Pantouvaki, J. Van Campenhout, R. Langer, and K. Barla, *Appl. Phys. Lett.* **109**, 091101 (2016).

<sup>25</sup>P. M. Petroff, A. C. Gossard, and W. Wiegmann, *Appl. Phys. Lett.* **45**, 620 (1984).

<sup>26</sup>L. Pfeiffer, K. W. West, H. L. Stormer, J. P. Eisenstein, K. W. Baldwin, D. Gershoni, and J. Spectra, *Appl. Phys. Lett.* **56**, 1697 (1990).

<sup>27</sup>E. Kapon, D. M. Hwang, and R. Bhat, *Phys. Rev. Lett.* **63**, 430 (1989).

<sup>28</sup>M. Kappelt, M. Grundmann, A. Krost, V. Türec, and D. Bimberg, *Appl. Phys. Lett.* **68**, 3596 (1996).

<sup>29</sup>C. S. Tsai, J. A. Lebens, C. C. Ahn, A. Nouhi, and K. J. Vahala, *Appl. Phys. Lett.* **60**, 240 (1992).

<sup>30</sup>S. Koshiba, H. Noge, H. Akiyama, T. Inoshita, Y. Nakamura, A. Shimizu, Y. Nagamume, M. Tsuchiya, H. Kano, H. Sakaki, and K. Wada, *Appl. Phys. Lett.* **64**, 363 (1994).

<sup>31</sup>C. Merckling, N. Waldron, S. Jiang, W. Guo, O. Richard, B. Douhard, A. Moussa, D. Vanhaeren, H. Bender, N. Collaert, M. Heyns, A. Thean, M. Caymax, and W. Vandervorst, *J. Appl. Phys.* **114**, 033708 (2013).

<sup>32</sup>H. S. Djie, C. L. Tan, B. S. Ooi, J. C. M. Hwang, X.-M. Fang, Y. Wu, J. M. Fastenau, W. K. Liu, G. T. Dang, and W. H. Chang, *Appl. Phys. Lett.* **91**, 111116 (2007).

<sup>33</sup>T. H. Gfroerer, *Photoluminescence in Analysis of Surfaces and Interfaces* (Wiley, Chichester, 2000).